

The Most Rapidly-Declining Type I Supernova 2019bkc/ATLAS19dqr

PING CHEN,^{1,2} SUBO DONG,¹ M. D. STRITZINGER,³ SIMON HOLMBO,³ JAY STRADER,⁴ C. S. KOCHANEK,^{5,6}
ERIC W. PENG,^{2,1} S. BENETTI,⁷ D. BERSIER,⁸ SASHA BROWNSBERGER,⁹ DAVID A. H. BUCKLEY,¹⁰ MARIUSZ GROMADZKI,¹¹
SHANE MORAN,^{12,13} A. PASTORELLO,⁷ ELIAS AYDI,⁴ SUBHASH BOSE,¹ THOMAS CONNOR,¹⁴ N. ELIAS-ROSA,^{15,16}
K. DECKER FRENCH,^{14,*} THOMAS W.-S. HOLOIEN,^{14,†} SEPPO MATTILA,¹² B. J. SHAPPEE,¹⁷ ANTONY A. STARK,¹⁸ AND
SAMUEL J. SWIHART⁴

¹*Kavli Institute for Astronomy and Astrophysics, Peking University, Yi He Yuan Road 5, Hai Dian District, Beijing 100871, China.*

²*Department of Astronomy, School of Physics, Peking University, Yi He Yuan Road 5, Hai Dian District, Beijing 100871, China*

³*Department of Physics and Astronomy, Aarhus University, Ny Munkegade 120, DK-8000 Aarhus C, Denmark*

⁴*Center for Data Intensive and Time Domain Astronomy, Department of Physics and Astronomy, Michigan State University, East Lansing, MI 48824, USA*

⁵*Department of Astronomy, The Ohio State University, 140 West 18th Avenue, Columbus, OH 43210, USA*

⁶*Center for Cosmology and AstroParticle Physics, The Ohio State University, 191 W. Woodruff Ave., Columbus, OH 43210, USA*

⁷*INAF - Osservatorio Astronomico di Padova, Vicolo dell'Osservatorio 5, I-35122 Padova, Italy*

⁸*Astrophysics Research Institute, Liverpool John Moores University, 146 Brownlow Hill, Liverpool L3 5RF, UK*

⁹*Department of Physics, Harvard University, Cambridge, MA 02138, USA*

¹⁰*South African Astronomical Observatory, PO Box 9, Observatory 7935, Cape Town, South Africa*

¹¹*Warsaw University Astronomical Observatory, Al. Ujazdowskie 4, 00-478 Warszawa, Poland*

¹²*Tuorla Observatory, Department of Physics and Astronomy, FI-20014, University of Turku, Finland*

¹³*Nordic Optical Telescope, Apartado 474, E-38700 Santa Cruz de La Palma, Spain*

¹⁴*The Observatories of the Carnegie Institution for Science, 813 Santa Barbara St., Pasadena, CA 91101, USA*

¹⁵*Institute of Space Sciences (ICE, CSIC), Campus UAB, Carrer de Can Magrans s/n, 08193 Barcelona, Spain*

¹⁶*Institut d'Estudis Espacials de Catalunya (IEEC), c/Gran Capitá 2-4, Edif. Nexus 201, 08034 Barcelona, Spain*

¹⁷*Institute for Astronomy, University of Hawaii, 2680 Woodlawn Drive, Honolulu, HI 96822, USA*

¹⁸*Center for Astrophysics — Harvard & Smithsonian, 60 Garden St.; Cambridge MA 02138 USA*

ABSTRACT

We report observations of the hydrogen- and helium-deficient supernova (SN) 2019bkc/ATLAS19dqr. With B - and r -band decline between peak and 10 days post peak of $\Delta m_{10}(B) = 4.9 \pm 0.1$ mag and $\Delta m_{10}(r) = 4.1 \pm 0.1$ mag, respectively, SN 2019bkc is the most rapidly-declining Type I SN discovered so far. The light curves and spectra of SN 2019bkc show some unprecedented characteristics compared to known SNe, while its closest matches are the rapidly-declining SN 2005ek and SN 2010X. SN 2019bkc appears “hostless”, with no identifiable host galaxy near its location, although it may be associated with the galaxy cluster MKW1 at $z = 0.02$. SN 2019bkc poses a challenge for existing models of fast-evolving SNe.

Keywords: supernovae: general – supernovae: individual: (SN 2019bkc/ATLAS19dqr)

1. INTRODUCTION

Modern wide-field time-domain surveys have significantly expanded the discovery space of the transient Universe, and in particular, surveys with higher cadences are finding an increasing number of rapid tran-

sients that rise and/or fall much faster than ordinary supernovae (SNe). A number of rapidly-evolving transients with spectroscopic data nominally belong to the H-deficient Type I SN class. Some well-studied examples include: SN 2002bj (Poznanski et al. 2010), SN 2010X (Kasliwal et al. 2010), SN 2005ek (Drout et al. 2013), OGLE-2013-SN-079 (Inserra et al. 2015) and iPTF 14gqr (De et al. 2018). These rapidly-evolving objects likely have small ejecta masses (\sim few tenths of M_{\odot}), and broadly speaking, they can be divided into those with He lines (e.g. SN 2002bj) and without (e.g.

Corresponding author: Subo Dong
dongsubo@pku.edu.cn

* Hubble Fellow

† Carnegie Fellow

SN 2010X), making them nominally Type Ib or Type Ic, respectively. In a few cases, fast-evolving transients show clear evidence of interaction with He-rich circumstellar material (e.g., Pastorello et al. 2015). Most of the known fast-evolving transients have been identified in large imaging surveys and lack spectroscopic follow-up (e.g., Drout et al. 2014; Rest et al. 2018). The theoretical interpretation of these fast-evolving SNe I is inconclusive, and include scenarios ranging from He-shell detonations on the surface of sub-Chandrasekhar mass white dwarf (WD) stars (the so-called SNe “Ia”; Bildsten et al. 2007; Shen et al. 2010) or possibly WDs that are disrupted in an accretion-induced collapse (AIC; see, e.g., Dessart et al. 2006; Tauris et al. 2013b); an ultra-stripped massive star explosion (see, e.g., Tauris et al. 2013a), core-collapse (cc) SNe with fallback (see, e.g., Moriya et al. 2010), or He-stars with an extended envelope (Kleiser & Kasen 2014), or being powered by magnetars (Yu et al. 2015).

Here we report observations of the rapidly-evolving Type I SN 2019bkc. SN 2019bkc exploded in an isolated environment and exhibited the most rapid post-peak photometric decline yet observed.

2. DISCOVERY

ATLAS19dqr/SN 2019bkc (RA= $10^h00^m22^s.544$, Dec= $-03^\circ01'12''.64$) was discovered by the Asteroid Terrestrial-impact Last Alert System (ATLAS; Tonry et al. 2018) on 2019 March 02.43 UT in the ALTAS “orange” filter at an apparent magnitude of $m_o = 17.96 \pm 0.06$ mag (Tonry et al. 2019). Following the practice of the ATLAS project we refer to the source as SN 2019bkc.

As can be seen in Fig. 1, SN 2019bkc is “hostless”, as no source is detected at its location down to $g \approx 24.3$ mag (5σ upper limit) in deep archived Dark Energy Camera Legacy Survey (DECaLS; Dey et al. 2019) DR7 images. It is located $217''$ from the cD galaxy NGC 3090 of the poor cluster MKW1 (Morgan et al. 1975). The averaged radial velocity of MKW1 members within an $0.5h^{-1}$ Mpc radius of NGC 3090 is 6252 ± 95 km s $^{-1}$ (Koranyi & Geller 2002), and we adopt $z = 0.0209 \pm 0.0003$ as the redshift of SN 2019bkc. Correcting for the infall velocity of the Local Group toward the Virgo Cluster yields a luminosity distance of $d_L = 86.5 \pm 4.3$ Mpc assuming a Λ CDM cosmology ($H_0 = 73$ km s $^{-1}$ Mpc $^{-1}$, $\Omega_m = 0.27$ and $\Omega_\Lambda = 0.73$) and $\sigma_{cz} = 300$ km s $^{-1}$ to account for peculiar velocities.

3. FOLLOW-UP OBSERVATIONS

We followed up 2019bkc as a candidate of a complete, magnitude-limited sample of ccSNe. We took the

first epoch of imaging on 2019 March 03.53 UT using 1-m Las Cumbres Observatory Global Telescope Network (LCOGT) telescope and the first spectrum using the 4.1-m Southern Astrophysical Research (SOAR) on 2019 March 05.27 UT. The peculiar SOAR spectrum and the rapid post-peak decline of the SN motivated us to carry out an extensive follow-up campaign of the SN. On 2019 March 06.44 UT, Prentice et al. (2019) reported a spectrum taken on 2019 March 04.92 UT and remarked that SN 2019bkc was an “unknown transient at an unknown redshift”. The extended Public ESO Spectroscopic Survey for Transient Objects (ePESSTO; Smartt et al. 2015) classified it as a likely SN Ic at $z \sim 0.04$ based a spectrum taken on 2019 March 06 UT (Carracedo et al. 2019).

We obtained optical/near-infrared (NIR) imaging with the 1-m LCOGT, the 1.3-m Small & Moderate Aperture Research Telescope System (SMARTS), the 3.8-m United Kingdom Infrared Telescope (UKIRT), the 2.56-m Nordic Optical Telescope (NOT), 2-m Liverpool Telescope (LT), and the 6.5-m Magellan telescopes. We detected SN from -1.4 d to $+40.2$ d relative to the epoch of B -band peak (see below). We obtained four visual-wavelength spectra on $+0.4$ d (SOAR), $+7.1$ d (The Southern African Large Telescope, SALT), $+7.1$ d (NOT), and $+10.1$ d (NOT), and all but the last one showed SN spectral features. Descriptions of the data acquisition and reduction are provided in Appendices A and B.

3.1. Light-curve evolution

We fit 3rd-order polynomials to the optical light curves (hereafter LCs) at $< +4$ d to measure the time and magnitude of the peak (see the best fits in Table 1). The B -band peak time (JD 2458547.4 ± 0.5 ; 2019 Mar 04.90 UT) is used as the reference epoch for the SN phase.

There was an ALTAS upper limit on -6.4 d at $m_o > 19.33$ mag preceding the -2.5 d detection (Tonry et al. 2019). Using Lasair (Smith et al. 2019), there was a detection on -5.6 d at $m_g = 18.69 \pm 0.11$ mag and a previous upper limit on -8.6 d of $m_g > 19.24$ mag from the Zwicky Transient Facility (ZTF; Bellm et al. 2019).

The g -band LC of SN 2019bkc (Fig. 2) rose by 1 mag to peak from detection in ~ 6 d. In contrast, the g -band flux dropped by ~ 2 mag by $+6$ d. In each optical band, between $\sim 4 - 10$ d, the LCs follow rapid exponential flux declines $f_\lambda \propto \exp(-t/\tau_{d,\lambda})$ with time scales $\tau_{d,\lambda} \approx 2$ d. We perform linear fits between $+4$ d and $+10$ d to determine post-peak decline rates (see Table 1). The decline rate is wavelength dependent, being faster in the bluer bands ($\tau_{d,B} = 1.73 \pm 0.05$ d or $0.63 \pm$

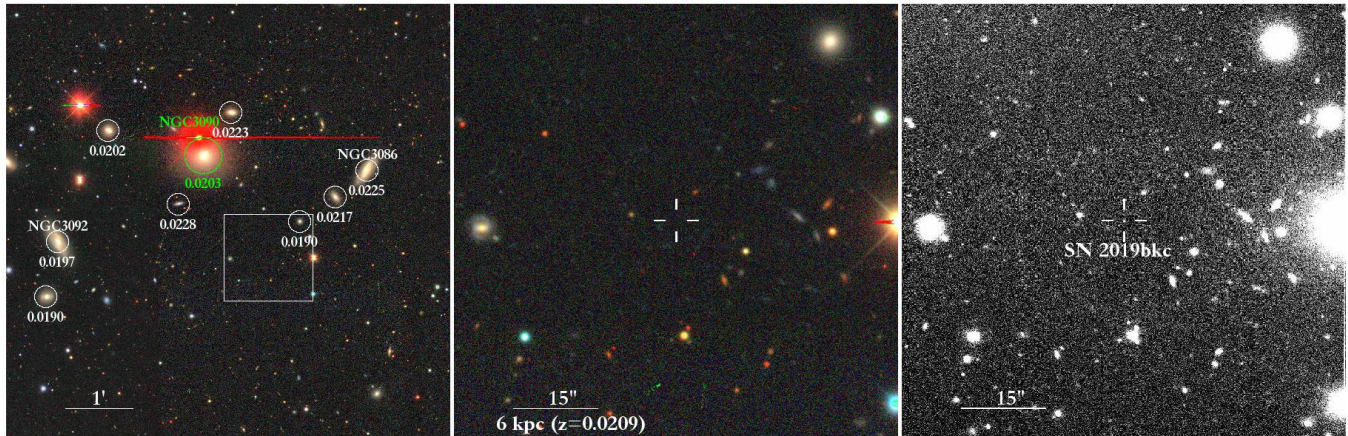


Figure 1. *Left:* Composite DECaLS (*grz*) image of the field of SN 2019bkc. The redshifts of the cD galaxy NGC 3090 along with NGC 3092, NGC 3086 and other members of the galaxy cluster MKW1 are labeled. *Middle:* Zoom in on the boxed region from the Left panel centered on SN 2019bkc whose position is indicated by the white cross. *Right:* A deep *i*-band NOT image of the same region including SN 2019bkc.

0.02 mag/d) than the redder bands ($\tau_{d,i} = 2.41 \pm 0.16$ d or 0.45 ± 0.03 mag/d). These decline rates are significantly faster than those of any previous rapidly-evolving SN I (see left panels of Fig. 2 and § 4.1). We have only sparse photometric coverage beyond $\sim +10$ d. Nevertheless, *i*-band images taken between $+16.3$ d and $+40.2$ d suggest the decline-rate became substantially slower at ≈ 0.07 mag/d.

We place an upper limit on the equivalent width (EW) of Na I D absorption at $z = 0.021$ of $< 0.4 \text{ \AA}$, which corresponds to $E(B - V)_{\text{host}} < 0.07$ mag (Phillips et al. 2013). Thus we assume no host reddening. Taking into account the Galactic extinctions of $E(B - V)_{\text{Gal}} = 0.06$ mag (Schlafly & Finkbeiner 2011) and $R_V = 3.1$, we compute the absolute peak magnitudes given in Table 1. At $M_r^{\text{peak}} = -17.3 \pm 0.1$ mag, SN 2019bkc is comparable to an average SN Ib/c (see, e.g. Taddia et al. 2018) and also the rapidly-declining SN 2005ek (Drout et al. 2013) and SN 2010X (Kasliwal et al. 2010); as shown in the right panel of Fig. 2 and discussion.

We constructed a pseudo-bolometric LC by performing black-body (BB) fitting (see Appendix A). At peak, SN 2019bkc reached $T_{\text{BB}} \approx 8,500$ K and $L_{\text{BB}} \approx 3 \times 10^{42}$ ergs/s.

3.2. Visual-wavelength Spectroscopy

Our spectra (Fig. 3) reveal a rapid evolution over one week. At peak the spectrum consists of a blue continuum with a number of broad absorption features. A week later the continuum is much redder, consistent with T_{BB} dropping from $\sim 8,500$ K to $\sim 4,000$ K, and shows substantial changes.

The spectral features of SN 2019bkc and their evolution do not have a good one-to-one match with any

existing SN, but there are similarities in multiple features with the rapidly-declining Type I SN 2010X and SN 2005ek, as well as with some Type Ic SNe, such as SN 2007gr (Valenti et al. 2008) aside from some velocity shifts (see Fig. 3 and § 4.1). We use these similarities to aid line identifications. Given the spectral peculiarities, we do not regard all these identifications as definitive, and the lines which are securely identified in 2007gr are marked in Fig. 3 as guidance.

In the first spectrum of SN 2019bkc, we identify a handful of prominent absorption features to measure their Doppler velocities at maximum absorption (v_{abs}). None of them shows a P-Cygni profile. They are attributed to Fe II $\lambda 5169$, Si II $\lambda 6355$, and C II $\lambda 6580$, and their v_{abs} values are $-9,461 \pm 182 \text{ km s}^{-1}$, $-12,896 \pm 253 \text{ km s}^{-1}$ and $-10,239 \pm 209 \text{ km s}^{-1}$, respectively. There is also a feature between $4200\text{--}4800 \text{ \AA}$, likely produced by a blend of ions including Fe, Ti and Mg.

A week past peak, the C II feature disappears, while the Fe II and possible Si II lines remain visible and show P-Cygni signatures. Furthermore, a feature at 5800 \AA emerges, along with a broad emission feature at 8500 \AA . The bluer feature is likely Na I $\lambda\lambda 5890, 5896$, while the latter feature is the Ca II NIR triplet.

The Fe II absorption velocity decreases to $v_{\text{abs}} \approx -2,545 \pm 275 \text{ km s}^{-1}$, with the caveat that the velocity measurement may be affected by significantly blended spectral features. The velocity of the possible Si II feature modestly decreases to $-11,756 \pm 525 \text{ km s}^{-1}$. Na I has a high $v_{\text{abs}} \approx -12,700 \pm 395 \text{ km s}^{-1}$ and for the Ca II triplet we find a lower limit of $v_{\text{abs}} \approx -5,196 \pm 229 \text{ km s}^{-1}$.

4. DISCUSSION

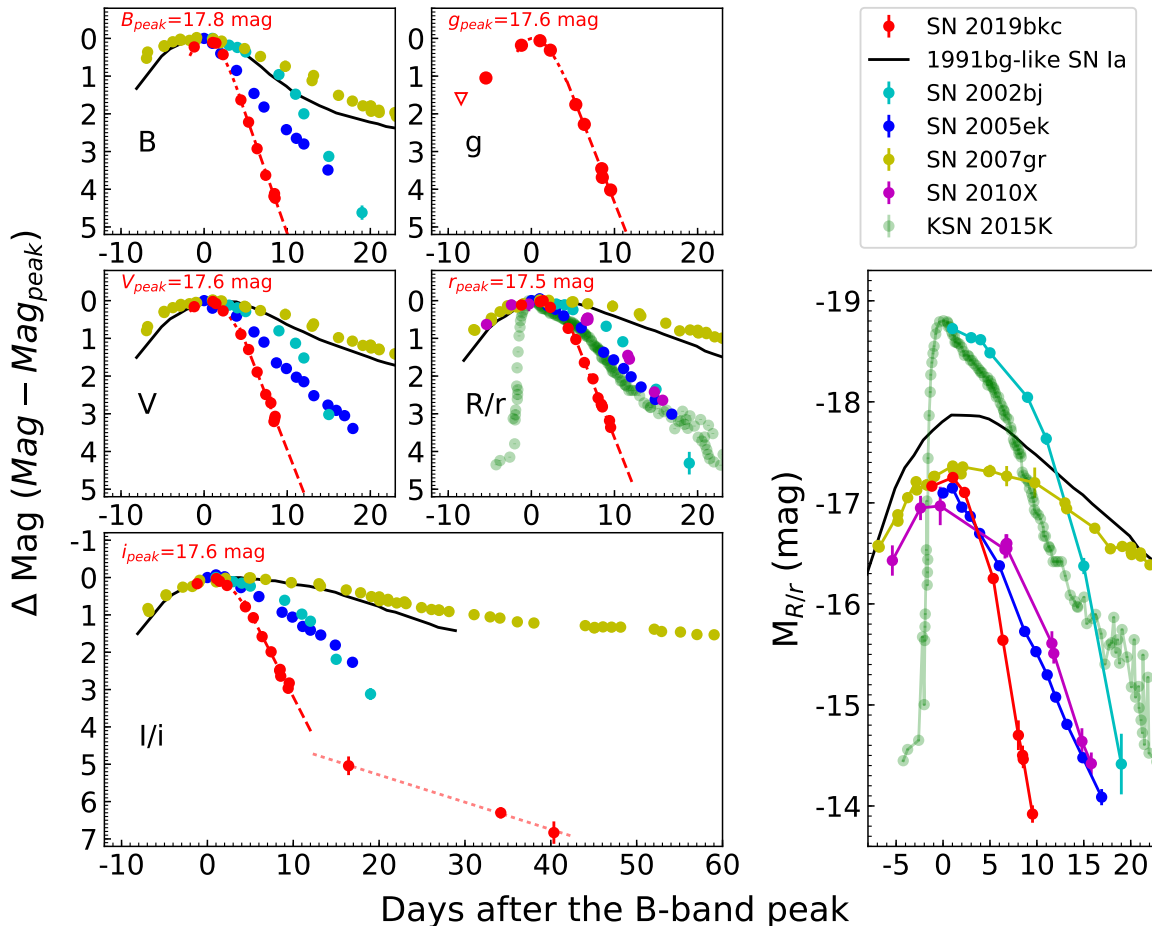


Figure 2. B -, V -, g -, R/r -, and I/i -band light curves (LCs) of SN 2019bkc compared with the fast-evolving Type I SNe 2002bj, 2005ek, and 2010X, the fastest-declining 1991bg-like Type Ia, the Type Ic SN 2007gr, and the fast transient KSN 2015K (in Kepmag) found by *Kepler*. The left panel normalizes the LCs to the peak brightness while the right panel shows the absolute R/r -band magnitudes. The dashed lines represent a low-order polynomial fit to the LCs of SN 2019bkc used to estimate the peak and decline-rate parameters in § 3.1. The dotted line is the best-fit straight line for the late-time i -band LC.

4.1. Comparison with known objects

In Fig. 2 we compare SN 2019bkc with several other rapidly-declining SNe with good photometric and spectroscopic coverage. The left panels show the optical LCs of SN 2019bkc normalized to the peak brightness compared to the rapidly-evolving SN 2002bj (Poznanski et al. 2010), SN 2005ek (Drout et al. 2013), SN 2010X (Kasliwal et al. 2010), and the fast transient KSN 2015K (Rest et al. 2018) found by *Kepler*. Also included are the LCs of the type Ic SN 2007gr (Valenti et al. 2008) and the 1991bg-like type Ia SN 1999by (Silverman et al. 2012).

SN 2019bkc declines faster than all of the SNe in the comparison sample. The decline between between peak

and +10 d for SN 2019bkc is $\Delta m_{10}(r) = 4.1 \pm 0.1$ mag, and for the previously known fastest-declining SNe it is $\Delta m_{10}(R) = 1.1 \pm 0.2$ mag for SN 2002bj, $\Delta m_{10}(R) = 1.85 \pm 0.15$ mag for SN 2005ek, $\Delta m_{10}(r) = 1.3 \pm 0.2$ mag for SN 2010X, and $\Delta m_{10}(\text{Kepmag}) = 2.1 \pm 0.03$ mag for KSN 2015K.

The right panel of Fig. 2 shows the absolute r/R -band magnitude evolution. SN 2005ek, SN 2010X and SN 2019bkc are the most similar, with peak absolute magnitudes ≈ -17 mag. The remainder of the comparison sample exhibits significant luminosity and/or luminosity evolution differences compared to SN 2019bkc at nearly all phases. In particular, SN 2002bj and

Table 1. Photometric parameters of SN 2019bkc

Filter	JD ^{peak}	$m_{\lambda}^{\text{peak}}$ (mag)	$M_{\lambda}^{\text{peak}}$ (mag)	$\Delta m_{10}(\lambda)^a$ (mag)	Decline Rate ^b (mag/day)
<i>B</i>	2458547.4 ± 0.5	17.77 ± 0.10	-17.14 ± 0.15	4.9 ± 0.2	0.63±0.02
<i>V</i>	2458547.7 ± 0.3	17.55 ± 0.05	-17.30 ± 0.12	4.4 ± 0.1	0.57±0.02
<i>g</i>	2458547.2 ± 0.5	17.64 ± 0.06	-17.25 ± 0.13	4.3 ± 0.1	0.56±0.02
<i>r</i>	2458547.6 ± 0.5	17.54 ± 0.03	-17.29 ± 0.11	4.1 ± 0.1	0.56±0.01
<i>i</i>	2458547.7 ± 0.5	17.57 ± 0.03	-17.25 ± 0.11	3.3 ± 0.1	0.45±0.03

^a The difference in magnitude between peak and +10 d.

^b As measured by a linear fit between +4 d and +10 d.

KSN 2015K are substantially more luminous (by $\gtrsim 1.5$ mag) at peak.

Of the comparison sample we find the spectra of SN 2005ek, SN 2010X and SN 2007gr are the most similar to SN 2019bkc. They all lack signatures of H and He (unlike SN 2002bj, which has He), and show features attributed to Fe II, Na I, Si II, C II, and Ca II. We have therefore chosen these three objects to show in in Fig. 3. SN 2019bkc’s line profiles are less pronounced than the comparison objects, especially post-peak Ca II, and it shows no clear signature of O I $\lambda 7773$. Given the spectral resemblance of these three rapidly-declining transients to SN 2007gr, they technically fall within the SN Ic sub-class.

There are significant differences in the absorption velocities between these SNe, which are reflected in the shifts adopted in Fig. 3. Most of the spectral features indicate that SN 2010X has the highest v_{abs} at $\gtrsim -12,000$ km s⁻¹ for most lines near peak. In comparison, SN 2005ek has Fe II and Si II $v_{abs} \sim -7,500$ km s⁻¹ at peak. At peak SN 2019bkc exhibits v_{abs} values between SNe 2005ek and 2010X, while its Fe II line drops more rapidly within a week (see § 3.2), although Na I and Si II still have high v_{abs} of ≈ -12000 km s⁻¹.

4.2. Interpretations

Next we discuss the possible energy sources and progenitor scenarios for SN 2019bkc.

The rapid LC evolution implies a low ejecta mass. For photon diffusion out of an expanding spherical ejecta with velocity $v = 10^4 v_4$ km s⁻¹, the optical depth is of the order $\tau \sim c/v$ when the diffusion time $t_{\text{diff}} = 4t_{\text{d4}}$ d equals to the time since explosion. The ejecta mass is approximately $M \sim 4\pi R^2/\kappa\tau \sim 0.08 M_{\odot} v_4 t_{\text{d4}}^2 \kappa_{0.3}^{-1}$, where $R = vt_{\text{diff}}$ and $\kappa = 0.3\kappa_{0.3}$ cm²/g is the ejecta opacity.

If the radiated energy is entirely from shock deposition (see, e.g. Waxman & Katz 2017), $E_{\text{rad}} \sim Mv^2 R_*/(2vt_{\text{diff}}) \sim Lt_{\text{diff}}$ and thus the progenitor radius $R_* \sim 5 \times 10^{12}$ cm, implying a massive star progenitor.

The remote location of SN 2019bkc implies an isolated progenitor (or in an un-detected globular cluster) in the outer galaxy halo or intracluster light, and it is thus probably associated with an old stellar population. The absence of a star-forming host galaxy down to $M_g \gtrsim -10.4$ and the non-detection of H α ($\lesssim 10^{37}$ erg s⁻¹ at $z = 0.021$) in our spectra make a massive star progenitor relatively unfavorable. However, we cannot completely rule out the possibilities of an extremely-low-luminosity dwarf-galaxy host, an isolated star forming region forming stars at $\lesssim 10^{-5} M_{\odot} \text{ yr}^{-1}$ or a hypervelocity runaway massive star from a nearby member of the MKW1 cluster (see Appendix C).

Next we consider whether the LCs can be solely ⁵⁶Ni-powered. We apply the integral relation of Katz et al. (2013) to the pseudo-bolometric LCs with low-order polynomial extrapolation to the explosion time (t_{exp}). Significant γ -ray escape from low-density ejecta can produce a fast decline, and we freely vary the γ -ray escape timescale t_0 (see Stritzinger et al. 2006, and references therein). We considered a broad range for t_{exp} , but find no satisfactory match with data. Therefore, energy deposition is unlikely to be dominated by ⁵⁶Ni decay.

Next we compare the pseudo-bolometric LCs of SN 2019bkc with the synthetic LCs predicted by various models. In the Ia scenario, a WD detonates from an accreted He layer (Bildsten et al. 2007), resulting in the production of $\lesssim 0.02 M_{\odot}$ of short-lived isotopes (e.g., ⁴⁸Cr, ⁵²Fe, ⁵⁶Ni) and the ejection of ~ 0.2 – $0.4 M_{\odot}$ of material (Shen et al. 2010). Alternative WD-related scenarios that produce short-lived transients include AIC of O/Ne/Mg WDs (e.g., Dessart et al. 2006; Tauris et al. 2013b). Several studies consider various types of evolved massive stars as possible progenitors of rapidly-declining SNe. Tauris et al. (2013a) modeled ultra-stripped ($\sim 1.5 M_{\odot}$) He-stars that explode following Fe-core collapse and reproduce the LC of SN 2005ek. (Moriya et al. 2010) studied dim ccSNe with fallback, in which a massive star ($\sim 13 M_{\odot}$) explodes with such low kinetic energy that only a small amount of material

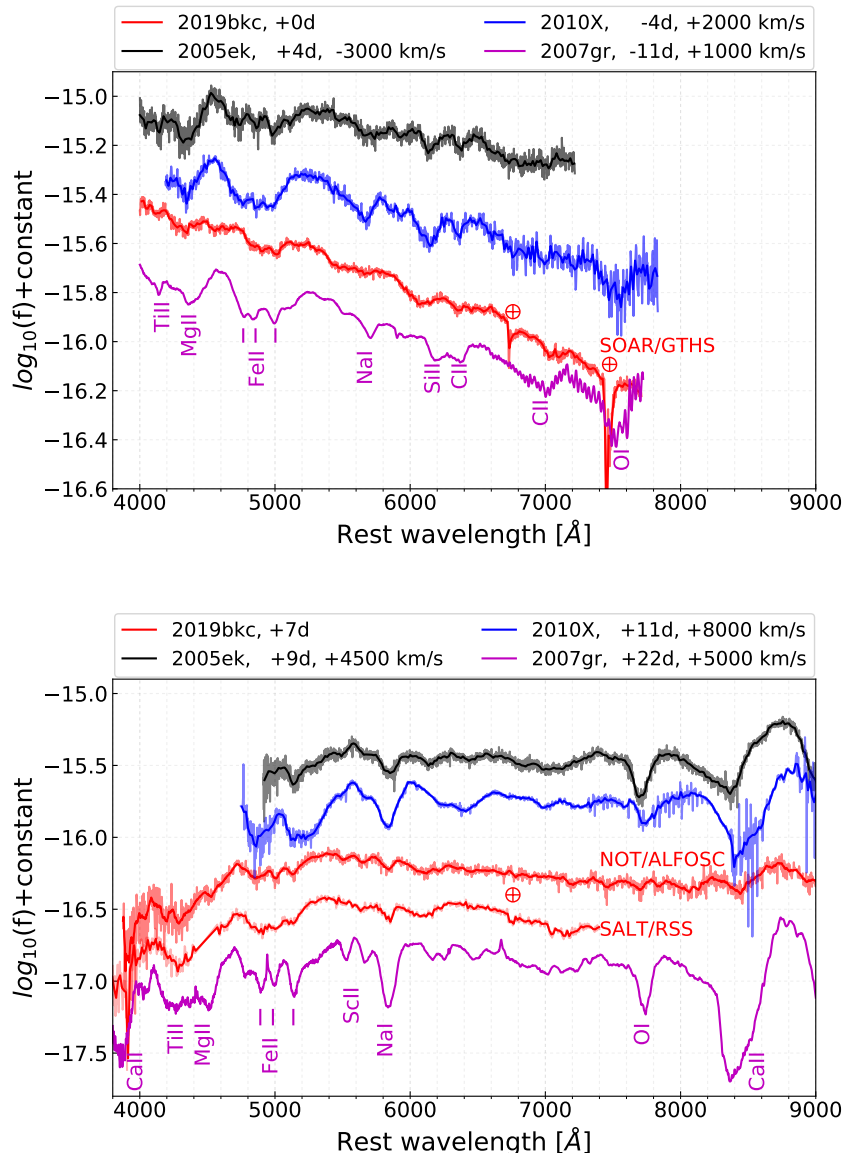


Figure 3. Visual-wavelength spectra of SN 2019bkc at peak (*top panel*) and +7 d (*bottom panel*) compared to similar phase spectra of the rapidly-declining SNe I 2005ek (Drout et al. 2013) and 2010X (Kasliwal et al. 2010), and the peculiar SN Ic 2007gr (Valenti et al. 2008). We apply wavelength shifts corresponding to the velocities indicated in each panel to the comparison objects to align the absorption features with SN 2019bkc. Specifically, the early-phase spectra of SN 2005ek, SN 2007gr and SN 2010X are shifted by $-3,000$ km s^{-1} , $+1,000$ km s^{-1} , and $+2,000$ km s^{-1} , respectively, while their post-peak spectra are shifted by $+4,500$ km s^{-1} , $+5,000$ km s^{-1} and $+8,000$ km s^{-1} .

(including ^{56}Ni) is ejected and the majority remains bound to a compact remnant. Kleiser & Kasen (2014) proposed explosion of $\sim 2\text{--}4 M_{\odot}$ He-stars with an extended envelope ($\gtrsim 25 R_{\odot}$) with no ^{56}Ni ejected to explain SN 2010X-like SNe, and the LC is powered by thermal energy deposited within the ejecta by the explosion shock wave following the core bounce (Dessart et al. 2011; Kleiser et al. 2018). Another possibility is

electron capture SNe (ECSNe) of $\approx 8 M_{\odot}$ AGB stars (e.g., Pumo et al. 2009; Moriya & Eldridge 2016).

The pseudo-bolometric LC of SN 2019bkc (including an estimate for > 15 d using the *i*-band-only data shown as open circles) is compared to these models in Fig. 4, and Appendix D gives the specific model parameters. Clearly none of the model LCs are able to reproduce the entire luminosity evolution of SN 2019bkc.

5. SUMMARY

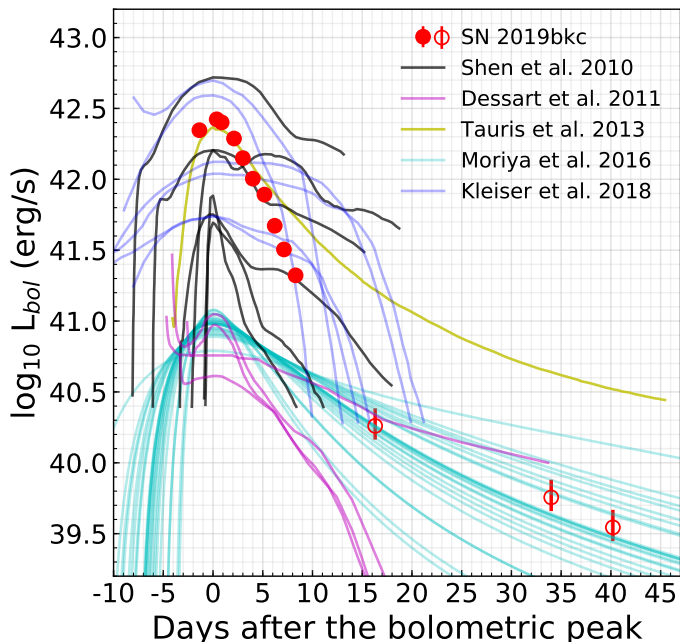


Figure 4. Pseudo-bolometric LC of SN 2019bkc, compared with synthetic LCs from various models. The open circles are estimated based on i -band LC at > 15 d. The models include: He-shell detonations (.Ia SNe; Shen et al. 2010), an ultra-stripped ccSN producing little ^{56}Ni (Tauris et al. 2013a), ccSNe of Wolf-Rayet stars producing no ^{56}Ni (Dessart et al. 2011), ^{56}Ni -free stripped ccSNe with circumstellar shells (Kleiser et al. 2018) and various ECSNe (Moriya & Eldridge 2016). See Appendix D for model parameters.

- SN 2019bkc is the most rapidly-declining SN I ever reported, and its unique LC evolution challenges all existing theoretical models for rapidly-declining transients.
- The spectra of SN 2019bkc lack H and He features and have some unprecedented characteristics. Some similarities are found with spectra of SN 2005ek and SN 2010X, which have comparable peak luminosities but slower post-peak decline rates. SN 2019bkc does not resemble the rapidly-declining SN 2002bj, which reached ~ 1.5 mag more luminous peak, contained He-lines in its spectrum, and had near-peak absorption line velocities a factor of two smaller than SN 2005ek, SN 2010X and SN 2019bkc.

- SN 2019bkc is “hostless” with no apparent host down to ~ -10.4 mag and likely exploded in an intracluster environment. This suggests a link with an older stellar population and disfavors massive star progenitors. SN 2019bkc suggests being cautious about assuming that fast declining “hostless” transients are Galactic, cataclysmic variable outbursts as is common in traditional SN classification programs.

We thank Boaz Katz, Konstantina Boutsia, Francesco Di Mille, Takashi Moriya and Thomas Tauris for their help. P.C., S.D. and S.B. acknowledge NSFC 11573003. We acknowledge Telescope Access Program (TAP) funded by the NAOC, CAS, and the Special Fund for Astronomy from the Ministry of Finance. M.S. and S.H. are supported by a project grant (8021-00170B) from the IRF, Denmark and a grant (13261) from VILLUM FONDEN. JS acknowledges support from the Packard Foundation. E.W.P. acknowledges NSFC. 11573002. EA acknowledge NSF grant AST-1751874. DAHB acknowledges South African National Research Foundation. MG is supported by the Polish NCN MAESTRO grant 2014/14/A/ST9/00121. KDF is supported by Hubble Fellowship grant HST-HF2-51391.001-A. SB is partially supported by the PRIN- INAF 2016 (P.I. M. Giroletti) SB and AAS acknowledge NSF grant AST-1814719. N.E.R. acknowledges Spanish MICINN grant ESP2017-82674-R and FEDER funds.

This work is partly based on NUTS observations made with NOT, operated by the NOT Scientific Association at the Observatorio del Roque de los Muchachos, La Palma, Spain, of IAC. ALFOSC is provided by IAA under a joint agreement with the University of Copenhagen and NOTSA. NUTS is funded in part by IDA. This paper includes data via Magellan Telescopes at LCO, Chile. This work is partly based on observations with SOAR, which is a joint project of the Ministério da Ciência, Tecnologia, Inovações e Comunicações (MCTIC) do Brasil, NOAO, UNC, and MSU. Some observations were obtained with SALT under the Large Science Programme on transients, 2018-2-LSP-001 (PI: DAHB). Polish support of this SALT programme is funded by grant no. MNiSW DIR/WK/2016/07.

REFERENCES

Bellm, E. C., Kulkarni, S. R., Graham, M. J., et al. 2019, *PASP*, 131, 018002

Bertin, E., Mellier, Y., Radovich, M., et al. 2002, in *Astronomical Society of the Pacific Conference Series*, Vol. 281, *Astronomical Data Analysis Software and Systems XI*, ed. D. A. Bohlender, D. Durand, & T. H. Handley, 228

- Bildsten, L., Shen, K. J., Weinberg, N. N., & Nelemans, G. 2007, *ApJL*, 662, L95
- Brown, W. R., Anderson, J., Gnedin, O. Y., et al. 2015, *ApJ*, 804, 49
- Carracedo, A. S., Barbarino, C., Brinnel, V., et al. 2019, *The Astronomer's Telegram*, 12555
- De, K., Kasliwal, M. M., Ofek, E. O., et al. 2018, *Science*, 362, 201
- Dessart, L., Burrows, A., Ott, C. D., et al. 2006, *ApJ*, 644, 1063
- Dessart, L., Hillier, D. J., Livne, E., et al. 2011, *MNRAS*, 414, 2985
- Dey, A., Schlegel, D. J., Lang, D., et al. 2019, *AJ*, 157, 168
- Drout, M. R., Soderberg, A. M., Mazzali, P. A., et al. 2013, *ApJ*, 774, 58
- Drout, M. R., Chornock, R., Soderberg, A. M., et al. 2014, *ApJ*, 794, 23
- Inserra, C., Sim, S. A., Wyrzykowski, L., et al. 2015, *ApJL*, 799, L2
- Kasliwal, M. M., Kulkarni, S. R., Gal-Yam, A., et al. 2010, *ApJL*, 723, L98
- Katz, B., Kushnir, D., & Dong, S. 2013, *ArXiv e-prints*, arXiv:1301.6766
- Kleiser, I., Fuller, J., & Kasen, D. 2018, *MNRAS*, 481, L141
- Kleiser, I. K. W., & Kasen, D. 2014, *MNRAS*, 438, 318
- Koranyi, D. M., & Geller, M. J. 2002, *AJ*, 123, 100
- Lang, D., Hogg, D. W., Mierle, K., Blanton, M., & Roweis, S. 2010, *The Astronomical Journal*, 139, 1782
- Liu, L.-D., Zhang, B., Wang, L.-J., & Dai, Z.-G. 2018, *ApJL*, 868, L24
- McConnachie, A. W. 2012, *AJ*, 144, 4
- Morgan, W. W., Kayser, S., & White, R. A. 1975, *ApJ*, 199, 545
- Moriya, T., Tominaga, N., Tanaka, M., et al. 2010, *ApJ*, 719, 1445
- Moriya, T. J., & Eldridge, J. J. 2016, *MNRAS*, 461, 2155
- Pastorello, A., Benetti, S., Brown, P. J., et al. 2015, *MNRAS*, 449, 1921
- Pellegrini, E. W., Oey, M. S., Winkler, P. F., et al. 2012, *ApJ*, 755, 40
- Phillips, M. M., Simon, J. D., Morrell, N., et al. 2013, *ApJ*, 779, 38
- Poznanski, D., Chornock, R., Nugent, P. E., et al. 2010, *Science*, 327, 58
- Prentice, S. J., Skillen, K., Maguire, K., Magee, M. R., & Clark, P. 2019, *Transient Name Server Classification Report*, 336
- Pumo, M. L., Turatto, M., Botticella, M. T., et al. 2009, *ApJL*, 705, L138
- Rest, A., Garnavich, P. M., Khatami, D., et al. 2018, *Nature Astronomy*, 2, 307
- Ryan-Weber, E. V., Meurer, G. R., Freeman, K. C., et al. 2004, *AJ*, 127, 1431
- Schechter, P. L., Mateo, M., & Saha, A. 1993, *PASP*, 105, 1342
- Schlafly, E. F., & Finkbeiner, D. P. 2011, *ApJ*, 737, 103
- Shen, K. J., Kasen, D., Weinberg, N. N., Bildsten, L., & Scannapieco, E. 2010, *ApJ*, 715, 767
- Silverman, J. M., Foley, R. J., Filippenko, A. V., et al. 2012, *MNRAS*, 425, 1789
- Skrutskie, M. F., Cutri, R. M., Stiening, R., et al. 2006, *AJ*, 131, 1163
- Smartt, S. J., Valenti, S., Fraser, M., et al. 2015, *A&A*, 579, A40
- Smith, K. W., Williams, R. D., Young, D. R., et al. 2019, *Research Notes of the American Astronomical Society*, 3, 26
- Smith, N., Cenko, S. B., Butler, N., et al. 2012, *MNRAS*, 420, 1135
- Stalder, B., Stark, A. A., Amato, S. M., et al. 2014, *the Proceedings of Ground-based and Airborne Instrumentation for Astronomy V*, 9147, doi:10.1117/12.2054933
- Stritzinger, M., Leibundgut, B., Walch, S., & Contardo, G. 2006, *A&A*, 450, 241
- Taddia, F., Stritzinger, M. D., Bersten, M., et al. 2018, *A&A*, 609, A136
- Tauris, T. M., Langer, N., Moriya, T. J., et al. 2013a, *ApJL*, 778, L23
- Tauris, T. M., Sanyal, D., Yoon, S.-C., & Langer, N. 2013b, *A&A*, 558, A39
- Tonry, J., Denneau, L., Heinze, A., et al. 2019, *Transient Name Server Discovery Report*, 310
- Tonry, J. L., Denneau, L., Heinze, A. N., et al. 2018, *PASP*, 130, 064505
- Valenti, S., Elias-Rosa, N., Taubenberger, S., et al. 2008, *ApJL*, 673, L155
- Waxman, E., & Katz, B. 2017, *Shock Breakout Theory*, ed. A. W. Alsabti & P. Murdin, 967
- Yu, Y.-W., Li, S.-Z., & Dai, Z.-G. 2015, *ApJL*, 806, L6

APPENDIX

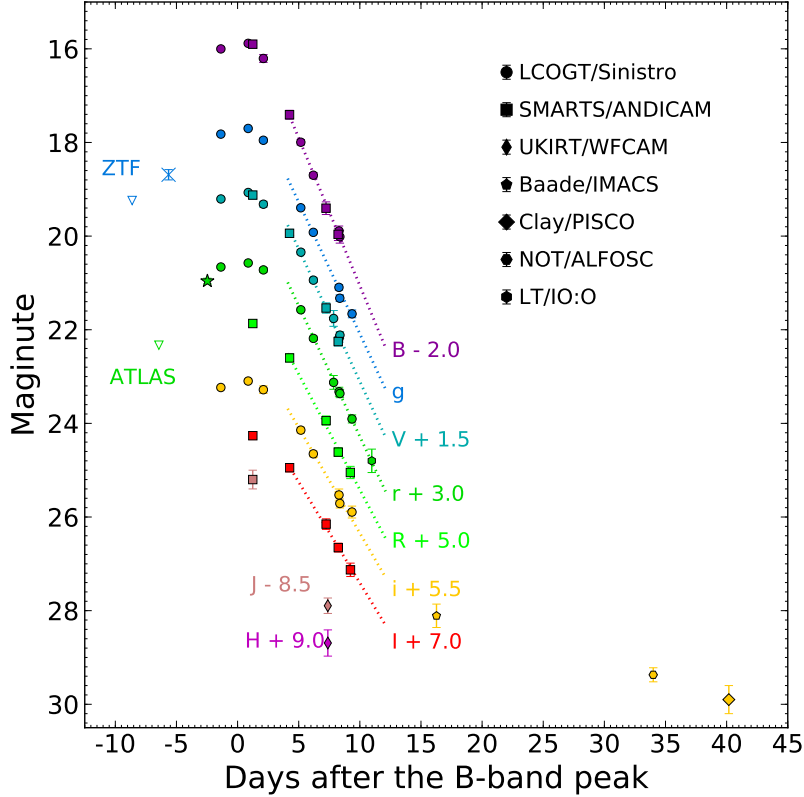


Figure 5. Multi-band LCs of SN 2019bkc. Dotted lines are linear fits to the data points between +4 d and +10 d. The upper limits from ATLAS and ZTF are shown with open down-pointing triangles.

A. PHOTOMETRY OBSERVATION, DATA AND SED

The majority of our optical images of SN 2019bkc were obtained with the LCOGT 1-m telescopes at Siding Spring Observatory (SSO), South African Astronomical Observatory (SAAO) and Cerro Tololo Interamerican Observatory (CTIO). Optical images were also taken with 1.3-m SMARTS +ANDICAM (A Novel Dual Imaging CAMera) at CTIO, the 2-m LT, and the 6.5-m Magellan telescopes. *J*-band data were obtained with SMARTS along with a single epoch of *JH*-band images from the Wide Field CAMera (WFCAM) on UKIRT. Most optical and NIR science images were reduced following standard procedures including bias/dark-frame and flat-field corrections, sky-subtraction, and the combination of multiple, dithered exposures. On the night of 2019 Apr 13 UT, using the Parallel Imager for Southern Cosmological Observations (PISCO) (Stalder et al. 2014), we acquired ten 120s simultaneous $\{g, r, i, z\}$ exposures of 2019bkc on the 6.5 – m Magellan/Clay telescope. We reduced these data using the standard PISCO Rapid Analysis Toolkit (Brownsberger19, in prep), and we briefly summarize this reduction procedure here. PISCO consists of four CCDs (one per band), and each CCD has two amplifiers. We apply an overscan correction to every amplifier for every image by subtracting from each amplifier a linear fit to the overscan pixels acquired as part of every readout. We median combine a stack of the eighteen overscan-corrected bias exposures acquired that night, and subtract the resulting ‘master bias’ from the flat and science images. We acquired forty-nine twilight flat images during our observations. However, not every flat can be used in the correction of every single-band CCD. We arrange the twilight flat image into four stacks, one for each band. A particular flat field is added to the stack for a particular band if

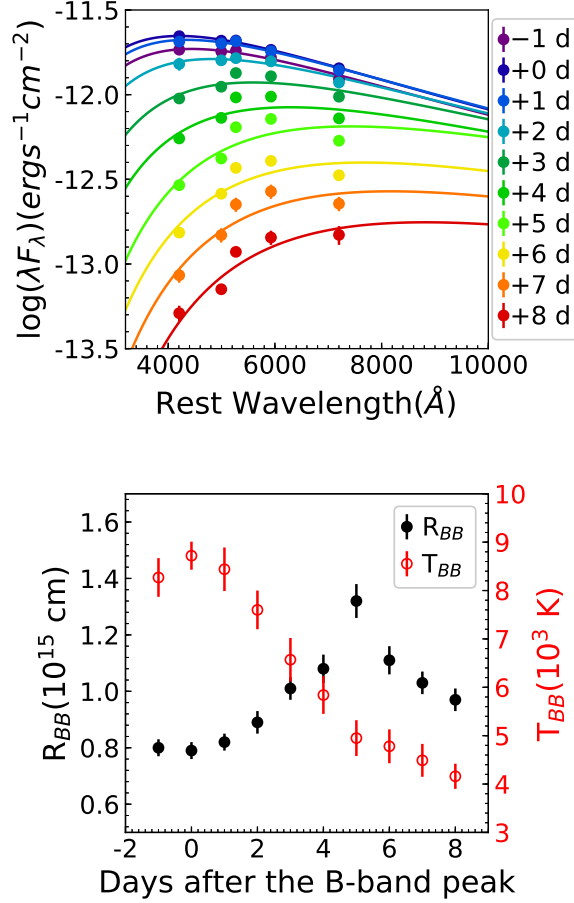


Figure 6. *Top:* SEDs constructed from our broad-band photometry. Over-plotted to each SED is the line corresponding to the best-fit BB function. *Bottom:* Time evolution of best-fit BB parameters: T_{BB} and R_{BB} .

and only if it has a characteristic surface brightness of between 5k and 15k ADU in that band, averaged between the two amplifiers. One flat can be placed into zero, one, or multiple single-band stacks. We normalize each overscan and bias corrected flat so that its median value is unity for the appropriate CCD, and then median combine each stack of normalized flats. We thus acquire a separate ‘maser flat’ field for each of the four PISCO filters. We overscan and bias correct each of the ten PISCO observations of 2019bkc, and separate each exposure into four single-band science images. We divide each of these forty single-band images by the appropriate master-flat. We use the plate-solution algorithm provided astrometry.net (Lang et al. 2010) to determine the World Coordinate System (WCS) solution for each image. We use this WCS solution and the SWarp coaddition software (Bertin et al. 2002) to produce our final PISCO $\{g, r, i, z\}$ images of 2019bkc.

Point-spread-function (PSF) photometry was computed with the DoPHOT (Schechter et al. 1993) package for all images except for the PISCO images, for which we performed aperture photometry. The optical band (Johnson B , V and Sloan r , i) photometry was calibrated relative to APASS photometry of stars in the field of the transient, while the NIR photometry was calibrated relative to 2MASS stars (Skrutskie et al. 2006). Template subtraction is not required to obtain a reasonable measure of the SN’s flux as there is no detectable host.

The optical spectral energy distribution (SEDs) shown in Fig. 6 were modelled as black-bodies (solid lines), in order to estimate (see bottom panel) the effective temperature (T_{BB}), and radius (R_{BB}) as a function of time. The R_{BB} evolution shows an initial increase from $\sim 0.8 \times 10^{15}$ cm up to $\sim 1.4 \times 10^{15}$ cm until +5 d, followed by a modest decline over the next several days, consistent with the typical radius evolution for the homologously expanding ejecta of a SN (see, e.g., Liu et al. 2018) rather than some other type of transients such as a Tidal Disruption Event. Following an

initial increase as the transient reaches peak brightness, both the luminosity and temperature subsequently decline as the ejecta expand and cool.

B. SPECTROSCOPIC OBSERVATION

The spectroscopic data were reduced and calibrated following standard procedures using IRAF. Each science spectrum was calibrated using a spectrophotometric standard observations. Finally, each spectrum was color-matched to the broad-band colors of SN 2019bkc.

Table 2. Journal of Spectroscopic Observation

Date	JD	Phase(d)	Range(Å)	Telescope Instrument
2019-03-05	2458547.77	0.4	3900-7900	SOAR/GTHS ^a
2019-03-11	2458554.45	7.1	3700-8300	SALT/RSS ^b
2019-03-11	2458554.53	7.1	4000-9700	NOT/ALFOSC ^c
2019-03-14	2458557.47	10.1	4000-9700	NOT/ALFOSC

^a Goodman High Throughput Spectrograph on SOAR. ^b Robert Stobie Spectrograph on SALT. ^c Alhambra Faint Object Spectrograph and Camera (ALFOSC) on NOT.

C. EXPLOSION ENVIRONMENT

Inspection of the Dark Energy Camera Legacy Survey (DECaLS; Dey et al. 2019) $g/r/z$ -band DR7 archival images (see Fig. 1) reveals no detectable sources at the position of SN 2019bkc. It is projected onto, and likely associated with, the poor cluster MKW1 (Morgan et al. 1975) (shown in the left panel of Fig. 1), which has a velocity dispersion of 367_{-54}^{+95} km s⁻¹ (Koranyi & Geller 2002). The cD galaxy of MKW1 is NGC 3090 and other prominent cluster members include NGC 3083, 3086, 3092, and 3101. Koranyi & Geller (2002) obtained a recessional velocity of $cz = 6089 \pm 35$ km s⁻¹ for NGC 3090 and an average velocity of $\bar{cz} = 6252 \pm 95$ km s⁻¹ for members within $0.5h^{-1}$ Mpc radius.

The projected distance of SN 2019bkc from NGC 3090 is 88.6 kpc (see Fig. 1). It is about 34 kpc from the closest known cluster-member galaxy ($z = 0.019$). SN 2019bkc is therefore likely located in the outer halo or is an intra-cluster source, where no recent star formation activity is expected to have occurred.

The 5σ g -band detection limit for the DECaL (Dey et al. 2019) is $g \approx 24.3$ mag, corresponding to $M_g \gtrsim -10.4^1$. At the distance of MKW1, $1''5 = 820$ pc, which means that a typical low-luminosity dwarf galaxy will have a size comparable to the seeing scale. From the Local Group dwarf galaxy compilation of McConnachie (2012), we find that nearly every gas-rich (i.e., star-forming) Local Group dwarf would be brighter than this limit only with KKR 3 ($M_V = -9.5$ mag) and Leo T ($M_V = -8$ mag) as exceptions. This absolute magnitude limit cannot rule out all but the most luminous globular clusters (GCs).

There is the possibility that SN 2019bkc resides in an isolated star forming region. H II regions in galactic outskirts are rare, but have been found associated with tidal H I features in the outskirts of gas-rich galaxies (Ryan-Weber et al. 2004). Although MKW1 does not appear to be a gas-rich environment, we can constrain the possibility of SN 2019bkc being in an isolated star-forming region. None of our spectra show discernible H α emission at the location of the SN, with an upper limit on the line flux of $\sim 10^{-17}$ erg s⁻¹ cm⁻² from the NOT/ALFOSC spectrum taken at +10 d. At the assumed distance of the SN, this translates into a maximum H α luminosity of $\sim 10^{37}$ erg s⁻¹, or a star formation rate of less than $10^{-5}M_{\odot}$ yr⁻¹. This is comparable to the luminosity of the Orion Nebula, whose ionizing flux is dominated by a single O star (Pellegrini et al. 2012). Although almost all ccSNe are associated with star forming regions, there are some notable exceptions such as SN 2010jp (Smith et al. 2012). This peculiar SN II was 33 kpc from its host center, and there is no detection of source in the pre-explosion image to a limiting absolute magnitude of ~ -12 .

A runaway star is a possible origin for a remote, massive star. However, given the ~ 30 Myr lifetime of a $\sim 10 M_{\odot}$ star, it would require a velocity $\gtrsim 1000$ km/s to travel the projected distance of 30 kpc to the closest member galaxy. Such a velocity is comparable to that of the fastest known hypervelocity star (e.g., Brown et al. 2015), which makes it an unlikely scenario.

¹ <http://legacysurvey.org/dr7/description/>

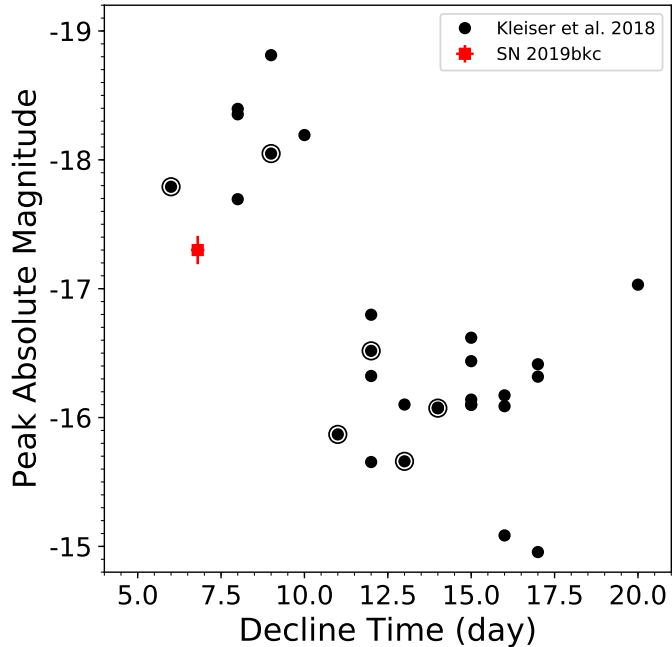


Figure 7. The r -band peak absolute magnitude and decline time of SN 2019bkc (red square) as compared to theoretical models (black dots) from Kleiser et al. (2018). The six models shown in Fig. 4 are circles and the decline time is defined by how long it takes for the r -band LC to decline in peak by two magnitudes.

We conclude that the lack of any obvious star-forming host galaxy and the non-detection of $H\alpha$ in the late-time spectrum make a massive star progenitor relatively unfavorable.

D. MODEL PARAMETERS

In this section, we describe the parameters of the model LCs shown in Fig. 4 and discussed in § 4.2.

Shen et al. (2010) studied the SNe Ia produced by the He detonation of material located on the surface of a WD which was accreted from a companion He-star. They adopted WD masses M_{WD} ranging from 0.6 to 1.2 M_{\odot} and envelope masses M_{env} from 0.02 to 0.3 M_{\odot} . Their predicted LCs are shown in black solid lines of Fig. 4. While some of the models can reach the peak luminosity of SN 2019bkc, they all decline too slowly compared to SN 2019bkc. The models decline more rapidly, have peak luminosities too dim, and rise times that are too fast compared to SN 2019bkc.

Dessart et al. (2011) presented fast-evolving ccSNe models from Wolf-Rayet progenitors when no ^{56}Ni is produced (models Bmi25mf6p49z1, Smi60mf7p08z1, Bmi25mf7p3z0p2 and Smi25mf18p3z0p05 in their Table 1 and 2). For these models, the final pre-explosion masses range from 6.49 to 18.3 M_{\odot} , and result from the evolution of 25 M_{\odot} or 60 M_{\odot} zero-age-main-sequence stars. All of the predicted LCs (shown in magenta in Fig. 4) are too dim at peak to explain SN 2019bkc.

Tauris et al. (2013a) studied ultra-stripped SNe Ic from close binary evolution and reproduced the bolometric light curve of SN 2005ek with $M_{cut} = 1.3M_{\odot}$, $E_{ej} = 5 \times 10^{50}$ and $M_{Ni} = 0.05 M_{\odot}$. As shown by the yellow solid line in Fig. 4, its predicted luminosity is similar to SN 2019bkc. Even though this is the model with the fastest post-decline rate from Tauris et al. (2013a), it is still too slow to explain SN 2019bkc.

Moriya & Eldridge (2016) studied rapidly-evolving dim transients from stripped-envelope electron-capture supernovae (ECSNe). In Fig. 4, we display the full collection of their models (solar metallicity $Z = 0.02$, type Ibc ECSN bolometric LCs), and of them are too dim compared to SN 2019bkc.

Kleiser et al. (2018) studied explosions of hydrogen-free massive stars where little or no radioactive nickel is ejected, and the source of radiation is almost all due to shock cooling. They explored a large parameter space of progenitor/explosion properties, including M_{shell} between 1 and 4 M_{\odot} , τ from 0.5 to 10 days, R_{mid} from 1 to 4×10^{12} cm

and E_{exp} covering $0.22 - 6 \times 10^{51}$ erg. For Fig. 4 we selected six models representing the six groups of models listed in their Table 1. We also show the r -band decline times and peak absolute magnitudes for all of their models in Fig. 7. The observed values for SN 2019bkc differ from the models, although some are relatively similar in these parameters. However, as shown in Fig. 4, these radioactive-free models all decline too fast at $\gtrsim +10 - 20$ d and so cannot explain the observed late-time slow decline of SN 2019bkc.